ACS APPLIED MATERIALS & INTERFACES

Research Article

www.acsami.org

Preparation–Morphology–Performance Relationships in Cobalt Aerogels as Supercapacitors

Geneva R. Peterson, Fernando Hung-Low, Cenk Gumeci, Will P. Bassett, Carol Korzeniewski, and Louisa J. Hope-Weeks*

Department of Chemistry and Biochemistry, Texas Tech University, Lubbock Texas 79409, United States

Supporting Information

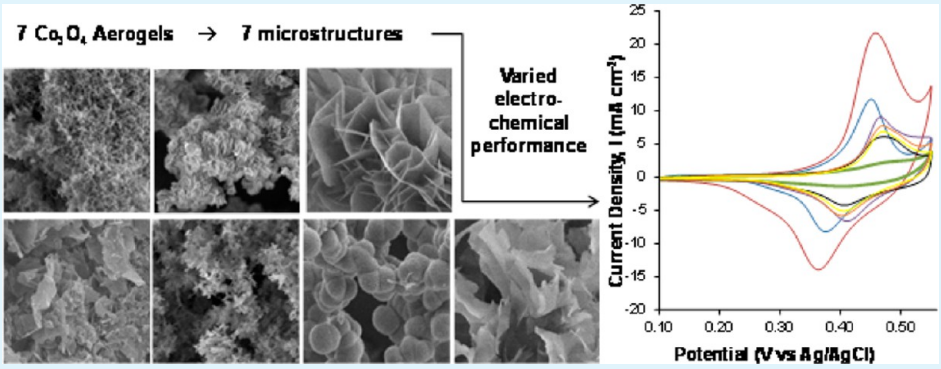

ABSTRACT: The ability to direct the morphology of cobalt sol–gel materials by using the simple synthetic parameters in epoxide-driven polycondensations has been dramatically demonstrated, and the influence of such morphological differences upon the supercapacity of the materials has been explored. Precursor salt, epoxide, and solvent all influence the speed of the sol–gel transition and the size and shape of the features observed in the as-prepared materials, thereby leading to highly varied microstructures including spheres, sponge-like networks, and plate assemblies of varied size. These morphological features of the as-prepared cobalt aerogels were observed for the first time by high resolution scanning electron microscopy (HRSEM). The as-prepared aerogel materials were identified by powder X-ray diffraction and thermogravimetry as weakly crystalline or amorphous cobalt basic salts with the general formula $Co(OH)_{2-n}X_n$ where X = Cl or NO_3 according to the precursor salt used in the synthesis. For all samples, the morphology was preserved through mild calcining to afford spinel phase Co_3O_4 in a variety of microstructures. Wide-ranging specific surface areas were determined for the as-prepared and calcined phases by physisorption analysis in agreement with the morphologies observed by HRSEM. The Co_3O_4 aerogels were evaluated for their supercapacitive performance by cyclic voltammetry. The various specimens exhibit capacitances ranging from 110 to 550 F g^{-1} depending upon the attributes of the particular aerogel material, and the best specimen was found to have good cycle stability. These results highlight the epoxide-driven sol–gel condensation as a versatile preparative route that provides wide scope in materials' properties and enables the analysis of structure–performance relationships in metal oxide materials.

KEYWORDS: *Co_3O_4, sol–gel, aerogel, cobalt oxide, spinel, supercapacitor*

1. INTRODUCTION

Considerable research effort has focused on the preparation of nanocrystalline spinel phases for use as electrocatalysts for the oxygen reduction reaction and as supercapcitors. Cobalt oxide-based systems[1−4] are of particular interest over the more expensive noble-metal alternatives such as iridium oxide.[5] But, like most ceramics, Co_3O_4 materials are challenging to prepare with sufficiently high surface areas to maximize electrochemical performance. Additionally, the ability to access a variety of physio-chemical attributes in solid-state nanomaterials and to evaluate the relationship between these attributes and materials' performance is an ongoing challenge in materials research. Clearly establishing the relationships between materials' preparation, the resulting properties, and their effectiveness in applications is essential for improved understanding of these systems and for acquisition of greener, more economic chemical technology.

Sol–gel chemistry provides a convenient route to inorganic nanomaterials with high chemical homogeneity, uniformity of physical properties, and high surface areas.[6] In general, these attributes may be accessed first by the formation of a sol–gel, then critical point drying to afford a high-surface area aerogel, and, if required, by calcining of the specimen to afford a metal oxide aerogel. In particular, the epoxide-driven sol–gel method has become a well-established route to a variety of high-surface area metal-oxide materials including CuO,[7] ZnO,[8] SnO_2,[9] and

Received: October 29, 2013
Accepted: January 13, 2014
Published: January 13, 2014

Co_3O_4,[1,10] among others. Because of the ease with which the preparative parameters in this sol−gel method may be varied, this synthetic approach allows the possibility to quickly generate libraries of materials specimens with varied properties.

In the epoxide-driven sol−gel approach, a concentrated metal salt solution is mixed with an epoxide that works as a proton scavenger, thereby irreversibly driving the polycondensation of metal hydrates to form μ-hydroxo and μ−oxo clusters which in turn grow to generate a continuous gel network (Figure 1). Key variables such as the precursor metal salt,[11] its

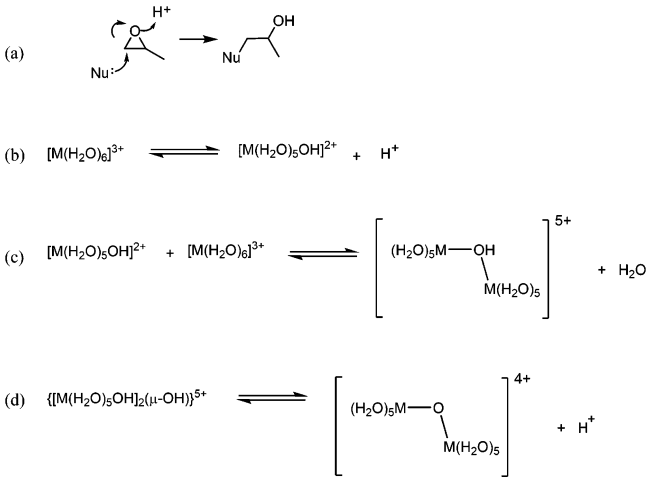

Figure 1. (a) Nonreversible scavenging of protons from the solution by epoxide ring-opening. The nucleophile may be the metal salt counterion or water, depending upon the polarity of the solvent and water content, and consequently the solvation of the anions. (b) Deprotonation of metal aquo complex. Note that other counterions may be present as inner sphere ligands depending on the solvent conditions. (c) Olation reaction to produce μ-hydroxo-bridged metal centers. (d) Oxolation to produce μ-oxo-bridged metal centers. This schematic shows the case for metals in 3+ oxidation state.

hydration state, the solvent, and the epoxide[12] can influence whether or not the system undergoes a gel transition or merely forms a precipitate. In the systems which do form gels, the above synthetic parameters may influence the physical properties of the resulting metal oxides such as their surface areas, morphology, and mechanical strength. The work reported herein provides a broad survey of gelation conditions for cobalt-based sol−gels that affords much improved conditions for faster, more robust cobalt materials. Furthermore, this work provides the first morphological investigation of cobalt sol−gel materials from epoxide-driven syntheses. Finally, we here illustrate an unprecedented level of variability in physical and chemical properties of the materials and discuss how these variations influence the observed electrochemistry.

In our hands, the two published methods[1,10] for generating cobalt oxide gels and aerogels via epoxide-driven polycondensation reactions either yield extremely fragile, difficult to handle materials[10] or gel slowly and incompletely.[1] This weak reactivity and structural integrity is not surprising, given that metals in the 2+ oxidation state generally gel less effectively and produce more fragile materials relative to higher oxidation state precursors due to the weak acidity of their metal hydroxide species in solution and the resulting sluggish oxolation and olation condensation steps necessary for the growth of a gel network. We have undertaken the current study to exploit the versatility of the epoxide-driven sol−gel synthesis of Co_3O_4 aerogels toward these goals: (1) to investigate the degree of influence exerted by different synthetic variables in these preparations, (2) to identify the conditions that will reliably afford cobalt sol−gels with improved physical and chemical properties, and (3) to examine the relationships between the resultant materials properties and their response in electrochemical potential cycling experiments that provide new insight in the design of next-generation supercapacitors.

2. EXPERIMENTAL SECTION

2.1. Syntheses. Cobalt nitrate hexahydrate, cobalt chloride hexahydrate, propylene oxide (PO), glycidol (GLY), epichlorohydrin (EPC), n-butylglycidyl ether (BGE), ethanol, 2-propanol, methanol, and ethylene glycol were all used as received. Epoxides were from Aldrich and solvents were from Fisher Scientific. (Caution: these epoxides and metal salts are toxic and/or carcinogenic). Alcogels were prepared in glass vials as molds (3 dram, 19 × 65 mm) under ambient conditions by the addition of epoxide (10 or 6 molar equivalents relative to Co^{2+}) to cobalt salt stock solutions (3.5 ml, 0.6 M). A table of the required volumes is given in Table S1 in the Supporting Information. After addition of the epoxide and brief mixing (ca. 10 s vortexing) the capped vials were allowed to stand undisturbed until stable gels had formed. Thereafter, the gels were washed in acetone baths over a week and then transferred to SPIDRY critical point driers. The solvent in the gels was exchanged with liquid CO_2. Typically, 5−6 gels were processed over 3−4 days, and then the extractor was brought beyond the critical point (38°C, 1100 psi) and vented slowly to ambient pressure over 6−8 h. As-prepared aerogels were calcined in a muffle furnace under static air by ramping the temperature to 300°C at a rate of 2 °C min^{-1}. The gels were held at 300°C for 2 h and then cooled to room temperature at a rate of 2°C min^{-1}.

2.2. Characterization. Powder X-ray diffraction (PXRD) patterns were collected on a Rigaku Ultima III diffractometer using Cu Kα radiation. Acquisition parameters for as-prepared specimens were varied in order to enhance signal-to-noise for these weakly crystalline materials. To qualitatively compare differences in crystallinity, calcined specimens were all analyzed under the following conditions: Bragg−Brentano geometry using a step width of 0.3° and a count time of 1 s; divergence and scattering slits were set at 2/3 and the receiving slit was set at 0.3.

Thermogravimetic analyses were carried out on a Shimadzu TA-50 instrument under a nitrogen flow rate of 50 mL min^{-1}. Aluminum sample pans were used and specimens weighed between one and two milligrams in all cases. The thermal program raised the specimens from room temperature to 100 °C at a rate of 10 °C min^{-1}, held at 100 °C for 1 h to remove residual adsorbed water, followed by a 5 °C min^{-1} ramp to 600 °C.

Physisorption data were collected on a Quantachome Nova 4200e instrument and analyzed with NovaWin 11.0 software. Nitrogen gas was used as the absorbate; equilibration times were 5 minutes. As-prepared aerogel specimens were degassed at 80 °C for 20 h and calcined specimens were degassed at 120 °C for 20 h. Brunauer Emmett Teller (BET) specific surface areas were determined from five data points in the relative pressure range of 0.05 and 0.3 P/P_0.

Scanning electron microscopy (SEM) was performed using a Hitachi 4300 scanning electron microscope. Each specimen was mounted on a 15 mm aluminum stub by dusting of the crumbled material onto carbon tape, followed by shaking off the excess. The specimens were sputter coated with Au−Pt at 10 V and 5 mA for 30 s. The materials were imaged at 2 kV using aperture 3 or 4, gun brightness of 1 or 2, and condenser lens setting of 13−16.

Electrochemical studies were conducted in a conventional three electrode glass cell using a potentiostat (PC4/300, Gamry Instruments, Warminster, PA). A 5 mm diameter glassy carbon disc electrode (Pine Research, Raleigh, NC) was used as the working electrode. A Pt wire and Ag/AgCl (3M KCl) served as the counter and the reference electrodes, respectively. Prior to each experiment, the glassy carbon electrode was polished to a mirror finish using a 0.05 μm alumina suspension, followed by rinsing in an ultrasonic cleaning bath

Table 1. Properties of Co-aerogel Specimens

specimen no.	synthetic precursors	gel time	mechanical quality	BET S.A. (m^2g^{-1}) as-prepared (calcined)	% S.A. reduction upon calcination	PXRD particle size of calcined specimens (nm)	capacitance ($F\ g^{-1}$)	capacitance per unit surface area ($F\ m^{-2}$)
1	$CoCl_2{\cdot}6H_2O$, MeOH, BGE	hours	stable	262 (71)	73	14	320	4.5
2	$CoCl_2{\cdot}6H_2O$, EtOH, BGE	3 days	very fragile	228 (93)	59	11	550	5.9
3	$Co(NO_3)_2{\cdot}6H_2O$, EtOH, BGE	hours	stable	91 (66)	27	13	259	3.9
4	$Co(NO_3)_2{\cdot}6H_2O$, MeOH, PO	10+ days	robust	142 (98)	31	10	282	2.9
5	$Co(NO_3)_2{\cdot}6H_2O$, MeOH, EPC	10+ days	robust	167 (83)	50	12	276	3.3
6	$Co(NO_3)_2{\cdot}6H_2O$, MeOH, BGE	10+days	fragile	147 (88)	40	11	268	3.0
7	$CoCl_2{\cdot}6H_2O$, IPA, GLY	hours	fragile	5 (28)		25	110	

filled with ultrapure water to remove alumina particles from the surface. A thin layer of Co_3O_4 aerogel material was formed on the glassy carbon electrode by dispensing a measured volume of the material's suspension. An aerogel suspension (10 mg of catalyst in 1 mL of ultrapure water) first was mildly sonicated for 15 min and then the homogenous ink solution subsequently was dispensed onto the glassy carbon electrode in 15 μL aliquots to yield 0.15 mg of Co_3O_4 aerogel (~0.77 mg $cm^{-2}_{(geo)}$) on the electrode.[13] This loading amount was found to be optimal (see Figure S7 in the Supporting Information). Higher loadings increased the sample thickness, thus hindering diffusion of the electrolyte into the internal pore surface of the material.

Cyclic voltammetry (CV) was applied in a 0.10−0.55 V potential window with various scan rates to probe aerogel super capacitor behavior. Measurements were conducted in 0.10 M KOH. Sample specific capacitance (C_s) was estimated from CV curves by integrating between 0.20−0.55 V. Electrochemical measurements were performed at room temperature (22 ± 1°C).

3. RESULTS AND DISCUSSION

3.1. Gel Formation Study. The general mechanism of the epoxide-addition sol−gel synthesis of transition metal gels is well-known:[11,12,14,15] the anion of a metal salt attacks an organic epoxide to open the epoxide ring. The resulting alcohol irreversibly scavenges protons from the solution, thereby mediating the pH of the solution and promoting the condensation polymerization of the hydrated metal cations to form a gel network. Successful acquisition of mesoporous gels (as opposed to condensed precipitates) relies on a gradual condensation polymerization. That is, the rate of all the various reaction steps needs to be in balance to allow the growth of a continuous three-dimensional polymer. Because the polarity of the solvent, the nucleophilicity of the metal anion, and the reactivity of the epoxide all influence the pH of the reaction medium and the rate of the condensation steps, we undertook a combinatorial approach to empirically identify conditions that rapidly and reliably afford stable cobalt sol−gels.

Two economical, soluble precursor salts, $CoCl_2{\cdot}6H_2O$ and $Co(NO_3)_2{\cdot}6H_2O$ were selected along with four solvents, ethanol, methanol, 2-propanol, and ethylene glycol. The concentration of metal salt in all solvents was held constant at 0.6 M. Four simple epoxides were also selected, propylene oxide, glycidol, n-butyl-gycidyl ether, and epichlorohydrin (structures shown in Tables S2 and S3 in the Supporting Information). As expected, preliminary screening showed that cobalt sols have a high tendency to form precipitates rather than gels, so the ratio of metal:epoxide was also varied. The traditional 1:10 molar ratio of metal:epoxide was used and also a ratio of 1:6 in the hope that reduced epoxide would lead to slower, more gradual condensation reactions and more stabilized gels. Altogether, these parameters generate 64 different conditions for the potential formation of cobalt sol−gels. In all but one case (specimen **7**), no macroscopic difference was noted in the sol−gels on the basis of metal:epoxide ratio, so excepting specimen **7**, the gels with 1:10 metal:epoxide were selected for further characterization. Complete details of the results of the sol−gel synthesis survey are given in Tables S2 and S3 in the Supporting Information.

Although most combinations of synthetic parameters resulted in precipitates or suspensions, seven conditions provided stable alcogels (specimens **1**−**7**) that were aged, washed with acetone, and subjected to critical point drying with carbon dioxide. Significant differences in gel time, color, and mechanical strength provided immediate qualitative indications of the variability of properties among these materials that were further examined through SEM, physisorption analyses, thermogravimetry, and PXRD. The properties of the resulting aerogels (photographs in Figures S1 and S2 in the Supporting Information) are shown in Table 1. Interestingly, three gels formed from $Co(NO_3)_2{\cdot}6H_2O$ in methanol, thereby providing a series in which the influence of epoxide could be examined. Notably, of 32 solvent−salt−epoxide combinations, seven successful sol−gel transitions were observed, and of these, four of them relied on n-butyl-glycidyl ether (BGE) as the epoxide, thus demonstrating the value of a quick exploration of synthetic parameters for a given metal when using the epoxide-addition method.

3.2. Phase Analysis of Co-aerogels. In all cases, the as-prepared aerogels exhibited poor crystallinity as observed by powder X-ray diffraction (Figure 2), indicating the amorphous nature and inexact stoichiometry of the as-prepared material (see Figure S3 in the Supporting Information for all as-prepared PXRD patterns). The PXRD patterns of as-prepared specimens **2**, **3**, and **7** closely resemble those of the cobalt basic salts of the general type $Co(OH)_{2-n}X_n$, where X is the counter ion of the precursor metal salt used in the sol−gel synthesis. The formation of cobalt basic salts is similar to the cases of

dx.doi.org/10.1021/am4047969 | ACS Appl. Mater. Interfaces 2014, 6, 1796−1803

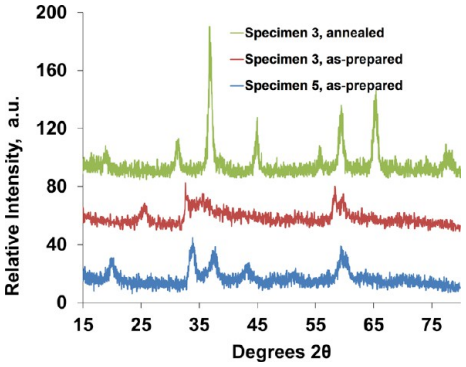

Figure 2. Representative PXRD patterns of Co-aerogel specimens corresponding to spinel Co_3O_4 after calcining (top) and the as-prepared, weakly crystalline cobalt basic salts (bottom).

epoxide-driven preparation of Ni[11] and Cu[7] sol–gels, which generate materials assigned as $Ni_3(OH)_4(NO_3)_2$ and $Cu_2(OH)_3Cl$, respectively. Cobalt basic salts are known to possess layered structures with variability of stoichiometry of both the hydroxide and ancillary anions as well as of intercalated water, thereby leading to a variety of colors of the bulk material including green, blue, lavender, and others.[16−18] This situation is observed in the sol–gel specimens reported here and accounts for the varied percent mass loss of these species upon thermal treatment (thermograms shown in Figure S5 in the Supporting Information). However, each specimen type reported here is homogenous throughout and its synthesis is reproducible.

The well-established thermogravimetric profiles for cobalt basic salts, $Co(OH)_2$,[19] $Co_2(OH)_3Cl$,[18,20] and $Co_2(OH)_3(NO_3)$[19,21] support the general assignment of these sol–gel materials as possessing the formula $Co(OH)_{2-n}X_n$ (X = Cl, NO_3). Specimens **3**, **4**, **5**, and **6**, which are derived from $Co(NO_3)_2$, all undergo a single, sharp mass loss between 220 and 230 °C corresponding to dehydroxylation of either $Co(OH)_3(NO_3)$ or $Co(OH)_2$. Specimen **1** shows a similar sharp mass loss, indicating similar behavior to $Co(OH)_2$. Specimens **2** and **7** undergo a two-step decomposition process consistent with the literature[20] for the $Co_2(OH)_3Cl$ phase, where the first mass loss corresponds to dehydroxylation to form $CoCl_2$ and CoO and the second mass loss corresponds to elimination of Cl_2. All of the as-prepared aerogel specimens afford Co_3O_4 upon calcining in air, as determined by PXRD (see Figure S4 in the Supporting Information for all PXRD patterns of the calcined aerogel materials). A previous study[1] examined the effects of optimizing the thermal calcining of a cobalt aerogel. Here, we desired to observe chemical and physical comparisons across a series of structurally different samples, so a consistent thermal treatment was adopted for all samples.

Examination of the PXRD patterns and thermograms demonstrates that solvent plays a key role in determining the as-prepared composition of the cobalt aerogels (Figure 2). Specimens **4**, **5**, and **6** were all prepared from $Co(NO_3)_2$ in methanol and display identical broad PXRD patterns and thermograms. In contrast, the PXRD pattern of specimen **3**, which is prepared from $Co(NO_3)_2$ in ethanol more closely resembles the $Co_2(OH)_3(NO_3)$ phase[19] and displays a slightly lower thermal decomposition onset. These observations suggest higher retention of the nitrate anion in this structure, which likely arises from the reduced polarity of the ethanol relative to the methanol, which in turn results in poorer solvation of the anionic nitrate in solution.

3.3. Microstructure and Morphology. Scanning electron microscopy of the aerogel specimens demonstrates the striking differences in microsctructure which are available by changing the gelation conditions (see Figures 3 and 4, see also additional images in the Supporting Information, pages S9–S22). Here it becomes apparent that the precursor salt plays the most significant role in directing the morphological habit of the aerogel structure, although the solvent and epoxide also influence the features. The gels prepared from $Co(NO_3)_2$ (Figure 3) all generate composites of platelike structures, although the size of these plates and the orderliness of their arrangement varies substantially with the solvent and epoxide. Three of the specimens (**4**, **5**, and **6**) were prepared in methanol, gelled slowly, and afforded large plate structures relative to the specimen **3** from ethanol, which gelled quickly, affording comparatively small florets of plates. One may reasonably implicate the reduced polarity of ethanol relative

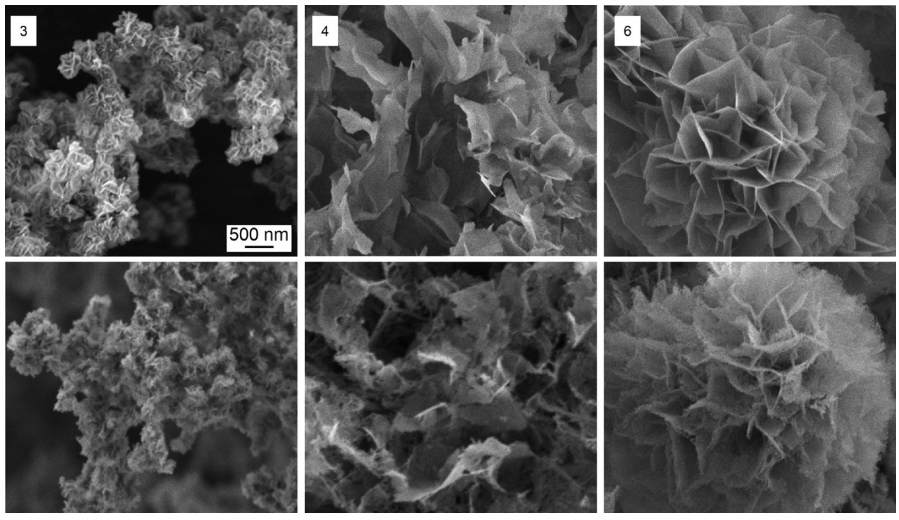

Figure 3. SEM of Co-aerogel specimens from $Co(NO_3)_2$. Top, as-prepared specimens; bottom, corresponding specimens after calcining. Note that specimen **5** (not shown here) displays similar morphology to Specimen **4** (additional images in the Supporting Information, pages S15–S16).

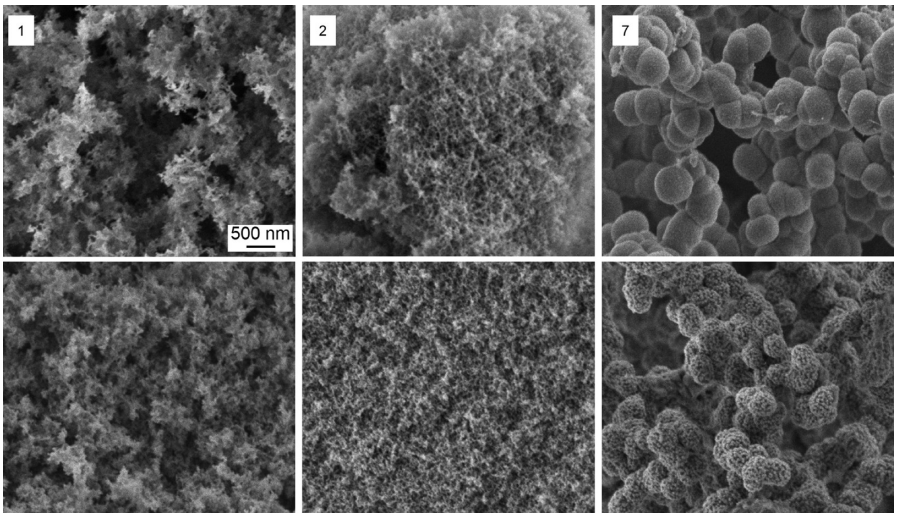

Figure 4. SEM of Co-aerogel specimens from $CoCl_2$. Top, as-prepared specimens; bottom, corresponding specimens after calcining.

to methanol in promoting faster nucleation of particles as a result of poorer solvation of the growing colloid precursors. This faster nucleation of particles gives rise to more numerous and smaller features, and a faster overall sol–gel transition (hours rather than days).

The gels derived from $CoCl_2$ (Figure 4) demonstrated alternative morphologies relative to the plate-structures of the $Co(NO_3)_2$ gels. For specimens **1** and **2** prepared from $CoCl_2$ using n-butylglycidyl ether (BGE) as the gelling agent, fine and homogeneous networks formed, a netlike web in the case of methanol and a flocculant sponge in the case of ethanol. In the case of specimen **7**, the morphology comprised large joined spheres. It is difficult to make direct comparisons with or rationalizations for specimen 7's features because no other conditions were identified in which stable Co gels formed using either 2-propanol or glycidol.

Physisorption data were collected to determine the BET specific surface areas of the aerogels, and the Scherrer equation was used to estimate the average particle size of the calcined aerogel samples from the most intense peak at approximately 37° 2θ. All specimens' average particle size fell between 11 and 25 nm. (Table 1). The as-prepared aerogels possess a wide range of surface areas in keeping with the varied morphologies observed in the SEM images. Calcining of the aerogel materials resulted in densification, coarsening, and reduction of surface areas for all specimens with the exception of specimen **7**, where an increase in specific surface area was noted after calcining. The SEM images of the calcined specimen **7** show roughening of the surface and possible pore-opening, as implicated in other cobalt aerogels that increased in surface area following calcining.[1] For the six specimens that underwent densification upon calcining, a direct relationship may be noted between the as-prepared surface area and the per cent reduction of surface area upon calcining. Specifically, the highest surface area material undergoes the most severe densification (specimen **1**, 73%), whereas the lowest surface area material undergoes the least densification (specimen **3**, 27%). These data follow intuitively, because higher surface area generally corresponds to greater mechanical fragility.

For all specimens, the morphological features of the as-prepared aerogels survived the calcining process, despite the densification and coarsening. The ability of different gelation conditions to afford noteworthy morphological differences in as-prepared aerogel materials should therefore be viewed as a mechanism to access varied microstructure in the functional phases even after calcining. Overall, the SEM, physisorption, and PXRD data all demonstrate the variability of materials properties resulting from simple changes in synthetic parameters. Because the microstructure of any heterogeneous system influences performance regardless of application, this structural variability arising from epoxide-driven syntheses of transition metal colloids provides wide scope for identifying synthetic routes for improved functional materials. Additional images for all specimens, as-prepared and calcined, are available in the the Supporting Information, pages S9–S22.

3.4. Electrochemistry. Results of cyclic voltammetry (CV) experiments carried out in 0.10 M KOH are reported in Figure 5. The waves between 0.3 V and 0.5 V are consistent with

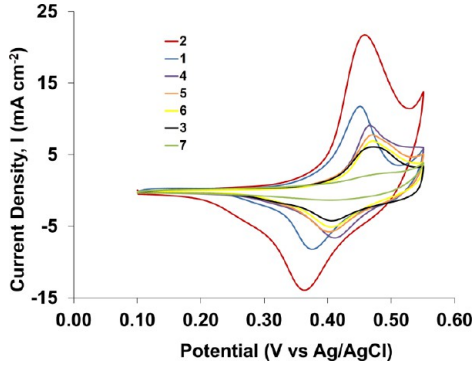

Figure 5. Cylic voltammograms of calcined Co_3O_4 aerogel samples in 0.1 M KOH recorded at 20 mV s^{-1} scan rate. The legend correlates to the sample numbers indicated in Table 1. The sample loading amount was 0.77 mg $cm^{-2}_{(geo)}$. Current densities are normalized to the geometric surface area of the glassy carbon electrode.

reports from earlier studies of Co_3O_4 materials,[22−26] and, for the aerogel materials under study here, can be attributed mainly to the following reactions

$$Co_3O_4 + OH^- + H_2O \rightarrow 3CoOOH + e- \quad (1)$$

$$CoOOH + OH^- \rightarrow CoO_2 + H_2O + e- \quad (2)$$

dx.doi.org/10.1021/am4047969 | ACS Appl. Mater. Interfaces 2014, 6, 1796−1803

The charge-transfer processes taking place across the region scanned in Figure 5 have been collectively ascribed to a pseudo-capacitive effect encompassing classical double layer contributions along with the various electron and ion transfer steps associated with the oxide forming reactions.[1,27−29] The former (classical double layer contributions) dominate at low potentials (0.1−0.3 V).

The detailed characteristics of the CVs in Figure 5 vary by sample. Comparison with Table 1 and Figure 3 and 4 indicates the responses depend mainly upon sample morphology and to some extent on BET surface area and crystallite size. For calcined specimens **1**−**6**, an effect of the anion (chloride versus nitrate) in the cobalt precursor salt also is evident. For example, $CoCl_2$ derived specimens **1** and **2** exhibit the highest current in the main voltammetric waves and greatest capacitance overall. In addition, relative to the other aerogels, which are $Co(NO_3)_2$ derived, the peaks associated with the eq 1 and 2 processes are shifted negative for specimens **1** and **2**. The differences suggest that the redox active $Co^{2+/3+/4+}$ sites in the aerogels prepared from $CoCl_2$ are more accessible to solvent and electrolyte ions needed for reaction and charge compensation than in the aerogels prepared from $Co(NO_3)_2$. As such, the capacitance per unit surface area (see Table 1) is higher for these specimens. This explanation seems consistent with the morphologies displayed in the SEM images. Figure 4 indicates gels prepared from the chloride precursors have a fine, homogeneous porous structure, in contrast to the dense plate structures that appear for the gels prepared from nitrate precursor. Having greater accessibility to the redox active sites reduces resistance to mass transport, which for specimens **1** and **2** can explain the shift of the redox waves for the eqs 1 and 2 reactions toward negative potentials, closer to the reversible potentials, and the increased charge storage capacity per gram of aerogel.

Because of the high pseudo-capacitance indicated for Specimen **2**, its properties were investigated further. Figure 6 shows effects of scan rate on the cyclic voltammetry. As the scan rate becomes greater, the current grows and the separation between anodic and cathodic waves increases. The changes in peak separation are affected by resistance to mass transport, as discussed above, but also likely are affected by sluggish reaction kinetics.

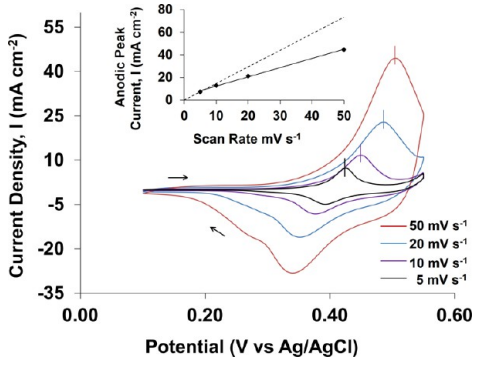

Figure 6. Cyclic voltammograms for specimen **2** (Table 1) recorded in 0.1 M KOH at the indicated scan rates. The sample loading and surface area reference are the same as mentioned in Figure 5. The vertical lines indicate the peak potentials (E_p) for the redox processes. Inset: Plot of peak current measured in the positive scan versus the scan rate. The solid line is derived from a straight line fit to the data points; the dashed line is the fit at slow scan rate that includes the plot origin.

For immobilized redox species undergoing reversible electron transfer reactions, the potential at the peak of the waves, E_p, coincides for both anodic and cathodic waves and remains fixed as scan rate varies.[30] However, E_p develops a dependency on scan rate as reaction kinetics slow.[31] The E_p shifts present in Figure 6 probably result from kinetic limitations associated with the reactions in eqs 1 and 2 together with resistance to the transport of OH^- ions through the aerogel matrix. The variation in charge passed at the different scan rates provides evidence for the latter contribution. The specific capacitance values calculated from the CVs in Figure 5 are 509, 592, 640, and 708 F g^{-1} at the scan rates of 50, 20, 10, and 5 mV s^{-1}, respectively. The tendency toward increasing capacitance at slow scan rates is typical of barriers within the aerogel pore structure, which become evident at the faster scan rates, and hinder the migration of ions in response to changes in the redox state of the metal centers.[27−29,32]

The inset in Figure 6 shows the changes in peak current with scan rate for the positive scans. The relationship is expected to be linear even for kinetically slow reactions.[33] The diminishing current at the highest scan rates, relative to the fit that includes the graph origin, is consistent with the trends in specific capacitance noted above, and probably results from restricted accessibility of solvent and ions to redox active sites within the aerogel matrix. Because the slope of the plot will depend upon the coverage of redox centers immobilized at the electrode,[34] the diminished current toward the higher scan rates reflects a decrease in the aerogel active surface area, or the area available for charge storage, on the measurement time scales employed.

Results of durability cycling are shown in Figure 7. After 500 cycles between −0.1 V and 0.52 V, the peak current near 0.5 V

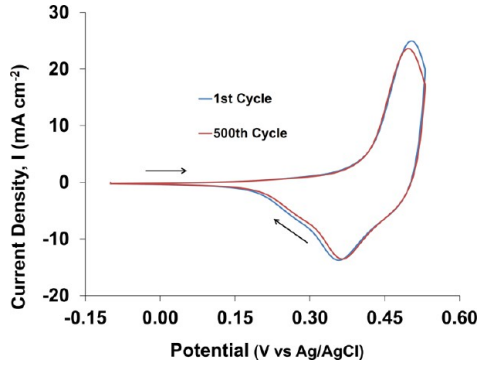

Figure 7. Voltammograms recorded before and just following durability cycling of Specimen **2** in 0.1 M KOH. The scan rate was 25 mV s^{-1}. The arrows show the scan direction.

on the positive scan is 98 % of the initial peak current in the region. Electrochemical durability is a critical parameter for the evaluation of potential supercapacitor materials in long-term applications. The amount of activity lost is small for the experimental conditions relative to other cobalt aerogels considered for use as charge storage materials in electrochemical capacitors.[1]

CONCLUSION

This article reports a comprehensive study of epoxide-driven preparations of cobalt sol gel nanomaterials as high surface area precursors for the industrially important spinel Co_3O_4 phase, and reveals the dramatically different properties that result from varied synthetic parameters. Seven conditions have been

identified for the reliable preparation of cobalt sol−gel materials, all of which serve as precursors for spinel Co_3O_4. Of four epoxides studied, n-butyl-glycidyl ether proved to have a high success rate in supporting the formation of stable cobalt sol-gels. Of the seven successful new gel conditions, one set of conditions (Specimen **1**) easily qualifies as the best in terms of speed of the sol−gel transition, mechanical robustness of the gel, and high surface area. Because the conditions under which a given metal salt successfully undergoes the sol−gel transition vary, the identification of multiple successful solvent−salt−epoxide combinations for cobalt sol−gel materials will inform and enable the identification of systems in which mixed-metal phases can be co-gelled as precursors for economical, functional cobalt spinel phases.[2]

Examination of the materials resulting from these varied sol−gel syntheses reveals a high degree of variability in the microstructure of these nanomaterials and corresponding variation in surface areas. This variability results from selection of the precursor metal salt, its solvent, and the epoxide gelation agent, in decreasing order of influence. All the materials derived from $Co(NO_3)_2$ produced platelet assembles on the microscale, whereas $CoCl_2$-derived materials generated two homogenous network morphologies, and one specimen consisting of joined microspheres. Solvent plays an important role in determining both the chemical and morphological nature of the resulting sol−gel materials. The use of a less polar solvent (i.e. ethanol, dielectric constant = 24.5) promotes faster sol−gel transitions, retention of counter ions in the gel network, and in one instance, smaller network features compared to a more polar solvent (i.e. methanol, dielectric constant = 33). All of these effects may be understood by the reduced solvation of the gel precursors by the lower-polarity solvent. Finally, the choice of epoxide seems to exert the least influence on the gel morphology, although it does strongly influence the likelihood of a successful sol−gel transition. All of the as-prepared microstructures including (spongelike, meshlike, small and large platelet assemblies, and spherical networks) were preserved through the calcining process. Consequently, the epoxide addition method for sol−gel synthesis should be viewed as a versatile means for the production of nanomaterial architectures.

The varied structures of the cobalt aerogels produced varied electrochemical performances with specific capacitances ranging from 110 to 550 F g^{-1}. The electrochemical performance of the different specimens was strongly influenced by morphology in addition to the intuitive influence of surface areas and particle sizes of the samples. This morphological influence highlights the value of the morphological variability available from the epoxide-driven sol−gel syntheses. Of all of the materials investigated, specimen **2** was further characterized electrochemically and was found to have high cycle durability and good performance at high sweep rates, indicating effective mass transport.

■ ASSOCIATED CONTENT

Supporting Information

Further synthetic details, aerogel photographs, experimental PXRD patterns, physisorption pore size distribution plots, thermogravimetric data, additional SEM images. This material is available free of charge via the Internet at http://pubs.acs.org.

■ AUTHOR INFORMATION

Corresponding Author

*E-mail: louisa.hope-weeks@ttu.edu.

Notes

The authors declare no competing financial interest.

■ ACKNOWLEDGMENTS

The authors are grateful for support received from the Office of Naval Research (N00014-11-1-0424) and the U.S. Department of Homeland Security (2008-ST-061-ED0001). Mark Grimson at the Texas Tech University Imaging Center is gratefully acknowledged for assistance with the scanning electron microscopy.

■ REFERENCES

(1) Wei, T. Y.; Chen, C. H.; Chang, K. H.; Lu, S. Y.; Hu, C. C. *Chem. Mater.* **2009**, *21*, 3228−3233.
(2) Wei, T. Y.; Chen, C. H.; Chien, H. C.; Lu, S. Y.; Hu, C. C. *Adv. Mater.* **2010**, *22*, 347−351.
(3) Cheng, F.; Shen, J.; Peng, B.; Pan, Y.; Tao, Z.; Chen, J. *Nat. Chem.* **2011**, *3*, 79−84.
(4) Liang, Y.; Li, Y.; Wang, H.; Zhou, J.; Wang, J.; Regier, T.; Dai, H. *Nat. Mater.* **2011**, *10*, 780−786.
(5) Hu, W.; Wang, Y.; Hu, X.; Zhou, Y.; Chen, S. *J. Mater. Chem.* **2012**, *22*, 6010−6016.
(6) Corriu, R., Anh, N. T. In *Molecular Chemistry of Sol−Gel Derived Nanomaterials*; Wiley: Chichester, U.K, 2009.
(7) Sisk, C. N.; Hope-Weeks, L. J. *J. Mater. Chem.* **2008**, *18*, 2607−2610.
(8) Gao, Y. P.; Sisk, C. N.; Hope-Weeks, L. J. *Chem. Mater.* **2007**, *19*, 6007−6011.
(9) Baumann, T. F.; Kucheyev, S. O.; Gash, A. E.; Satcher, J. H. *Adv. Mater.* **2005**, *17*, 1546−1548.
(10) Gill, S. K.; Shobe, A. M.; Hope-Weeks, L. J. *Scanning* **2009**, *31*, 132−138.
(11) Gash, A. E.; Satcher, J. H.; Simpson, R. L. *J. Non-Cryst. Solids* **2004**, *350*, 145−151.
(12) Gash, A. E.; Tillotson, T. M.; Satcher, J. H.; Poco, J. F.; Hrubesh, L. W.; Simpson, R. L. *Chem. Mater.* **2001**, *13*, 999−1007.
(13) Davis, M.; Gumeci, C.; Black, B.; Korzeniewski, C.; Hope-Weeks, L. *RSC Advances* **2012**, *2*, 2061−2066.
(14) Gash, A. E.; Tillotson, T. M.; Satcher, J. H.; Hrubesh, L. W.; Simpson, R. L. *J. Non-Cryst. Solids* **2001**, *285*, 22−28.
(15) Laberty-Robert, C.; Long, J. W.; Lucas, E. M.; Pettigrew, K. A.; Stroud, R. M.; Doescher, M. S.; Rolison, D. R. *Chem. Mater.* **2006**, *18*, 50−58.
(16) Liu, Z.; Ma, R.; Osada, M.; Takada, K.; Sasaki, T. *J. Am. Chem. Soc.* **2005**, *127*, 13869−13874.
(17) Ramesh, T. N.; Rajamathi, M.; Vishnu Kamath, P. *J. Solid State Chem.* **2006**, *179*, 2386−2393.
(18) Zhao, Z.; Geng, F.; Bai, J.; Cheng, H.-M. *J. Phys. Chem. C* **2007**, *111*, 3848−3852.
(19) Ramesh, T. N. *J. Solid State Chem.* **2010**, *183*, 1433−1436.
(20) Garciamartinez, O.; Millan, P.; Rojas, R. M.; Torralvo, M. J. *J. Mater. Sci.* **1988**, *23*, 1334−1350.
(21) Markov, L.; Petrov, K.; Petkov, V. *Thermochim. Acta* **1986**, *106*, 283−292.
(22) Keng, P. Y.; Kim, B. Y.; Shim, I.-B.; Sahoo, R.; Veneman, P. E.; Armstrong, N. R.; Yoo, H.; Pemberton, J. E.; Bull, M. M.; Griebel, J. J.; Ratcliff, E. L.; Nebesny, K. G.; Pyun, J. *ACS Nano* **2009**, *3*, 3143−3157.
(23) Tummala, R.; Guduru, R. K.; Mohanty, P. S. *J. Power Sources* **2012**, *209*, 44−51.
(24) Hu, C.-C.; Hsu, T.-Y. *Electrochim. Acta* **2008**, *53*, 2386−2395.
(25) Wang, X.; Sumboja, A.; Khoo, E.; Yan, C.; Lee, P. S. *J. Phys. Chem. C* **2012**, *116*, 4930−4935.

(26) Vijayakumar, S.; Ponnalagi, A. K.; Nagamuthu, S.; Muralidharan, G. *Electrochim. Acta* **2013**, *106*, 500−505.
(27) Xia, X.-H.; Tu, J.-P.; Wang, X.-L.; Gu, C.-D.; Zhao, X.-B. *Chem. Commun.* **2011**, *47*, 5786−5788.
(28) Meher, S. K.; Rao, G. R. *J. Phys. Chem. C* **2011**, *115*, 25543−25556.
(29) Meher, S. K.; Rao, G. R. *J. Phys. Chem. C* **2011**, *115*, 15646−15654.
(30) Bard, A. J., Faulkner, L. R. In *Electrochemical Methods: Fundamenals and Applications*, 2nd ed.; John Wiley & Sons: New York, 2001; pp 590−594.
(31) Bard, A. J., Faulkner, L. R. In *Electrochemical Methods: Fundamenals and Applications*, 2nd ed.; John Wiley & Sons: New York, 2001; pp 591, 594.
(32) Simon, P.; Gogotsi, Y. *Nat. Mater.* **2008**, *7*, 845−854.
(33) Bard, A. J., Faulkner, L. R. In *Electrochemical Methods: Fundamenals and Applications*, 2nd ed.; John Wiley & Sons, Inc.: New York, 2001; p 589−591.
(34) Bard, A. J., Faulkner, L. R. In *Electrochemical Methods: Fundamenals and Applications*, 2nd ed.; John Wiley & Sons, Inc.: New York, 2001; p 591.